AGU PUBLICATIONS

Geophysical Research Letters

RESEARCH LETTER
10.1002/2016GL069446

Key Points:
- Large areas of forecasted stronger turbulence over the western U.S. mountainous regions are reduced by additional terrain averaging
- Unphysical energy spectra induced by unfiltered small-scale (~2Δx) topography are damped out in the initialization of the model
- Reducing unphysical mountain-wave-like features significantly improves operational turbulence forecasts over the mountain region

Correspondence to:
J.-H. Kim,
jung-hoon.kim@noaa.gov;
jhkim99@me.com

Citation:
Park, S.-H., J.-H. Kim, R. D. Sharman, and J. B. Klemp (2016), Update of upper level turbulence forecast by reducing unphysical components of topography in the numerical weather prediction model, *Geophys. Res. Lett.*, *43*, 7718–7724, doi:10.1002/2016GL069446.

Received 4 MAY 2016
Accepted 6 JUL 2016
Accepted article online 11 JUL 2016
Published online 26 JUL 2016

Update of upper level turbulence forecast by reducing unphysical components of topography in the numerical weather prediction model

Sang-Hun Park[1], Jung-Hoon Kim[2,3], Robert D. Sharman[4], and Joseph B. Klemp[1]

[1]Mesoscale and Microscale Meteorology Laboratory, National Center for Atmospheric Research, Boulder, Colorado, USA, [2]Cooperative Institute for Research in the Atmosphere/Colorado State University (CIRA/CSU), Fort Collins, Colorado, USA, [3]Aviation Weather Center, NOAA, Kansas City, Missouri, USA, [4]Research Application Laboratory, National Center for Atmospheric Research, Boulder, Colorado, USA

Abstract On 2 November 2015, unrealistically large areas of light-or-stronger turbulence were predicted by the WRF-RAP (Weather Research and Forecast Rapid Refresh)-based operational turbulence forecast system over the western U.S. mountainous regions, which were not supported by available observations. These areas are reduced by applying additional terrain averaging, which damps out the unphysical components of small-scale (~2Δ*x*) energy aloft induced by unfiltered topography in the initialization of the WRF model. First, a control simulation with the same design of the WRF-RAP model shows that the large-scale atmospheric conditions are well simulated but predict strong turbulence over the western mountainous region. Four experiments with different levels of additional terrain smoothing are applied in the initialization of the model integrations, which significantly reduce spurious mountain-wave-like features, leading to better turbulence forecasts more consistent with the observed data.

1. Introduction

Unexpected turbulence encounters at cruising altitudes of $z = 8 \sim 12$ km are a leading cause of weather hazards for the aviation industry and may cause in-flight injuries, flight delays, and structural damage [e.g., *Sharman et al*., 2012]. Turbulence in the absence of adjacent deep convection is normally referred to as Clear-Air Turbulence, which often occurs near the upper level jet and frontal system due to shear instability, inertial instability, and geostrophic adjustment or spontaneous imbalance [e.g., *Endlich*, 1964; *Dutton and Panofsky*, 1970; *Shapiro*, 1980; *Ellrod and Knapp*, 1992; *Knox et al*., 2008; *Kim et al*., 2016]. Upper level turbulence can also occur over the complex mountainous regions mainly due to the interactions between mountain waves and the background wind, which is known as mountain-wave turbulence (MWT) [e.g., *Lane et al*., 2009; *Kim and Chun*, 2010, 2011; *Sharman et al*., 2011].

Upper level turbulence directly affecting aircraft has roughly 10–1000 m horizontal wavelengths [e.g., *Sharman et al*., 2006; *Kim et al*., 2015], which are still subgrid scale in current operational Numerical Weather Prediction (NWP) models, although horizontal and vertical resolutions are continually improving with increased computing power. Detection of upper level turbulence using onboard radar or lidar systems is still not adequate to provide guidance for tactical turbulence avoidance. Operational turbulence forecasts are provided by the Graphical Turbulence Guidance (GTG) [*Sharman et al*. [2006], *Kim et al*. [2011]), which uses operational NWP model output as an input to infer a magnitude of atmospheric turbulence in terms of an eddy dissipation rate (EDR; $m^{2/3} s^{-1}$) by assuming that the resolved-scale energy in the model cascades down to smaller-scale eddies directly affecting cruising aircraft [e.g., *Lindborg*, 2007]. Therefore, this turbulence forecast system is highly dependent upon the configuration and performance of the underlying NWP model. The GTG uses the operational Weather Research and Forecast Rapid Refresh (WRF-RAP) [*Benjamin et al*., 2016] system based on WRF [*Skamarock et al*., 2008] NWP model.

It has been demonstrated that increasing horizontal and vertical resolutions can help reproduce realistic values of turbulence magnitude and location in case study simulations [e.g., *Lane et al*., 2012; *Kim and Chun*, 2010, 2012; *Kim et al*., 2014, 2015; *Trier and Sharman*, 2009; *Trier et al*., 2010, 2012]. In spite of recent increases in operational NWP model resolution, end users from commercial airlines have been reporting that the turbulence forecasts tend to overestimate smooth-to-light turbulence to be light-or-stronger turbulence especially over the western mountainous region of U.S. (M. A. Thomas, personal communication, 2016). As an

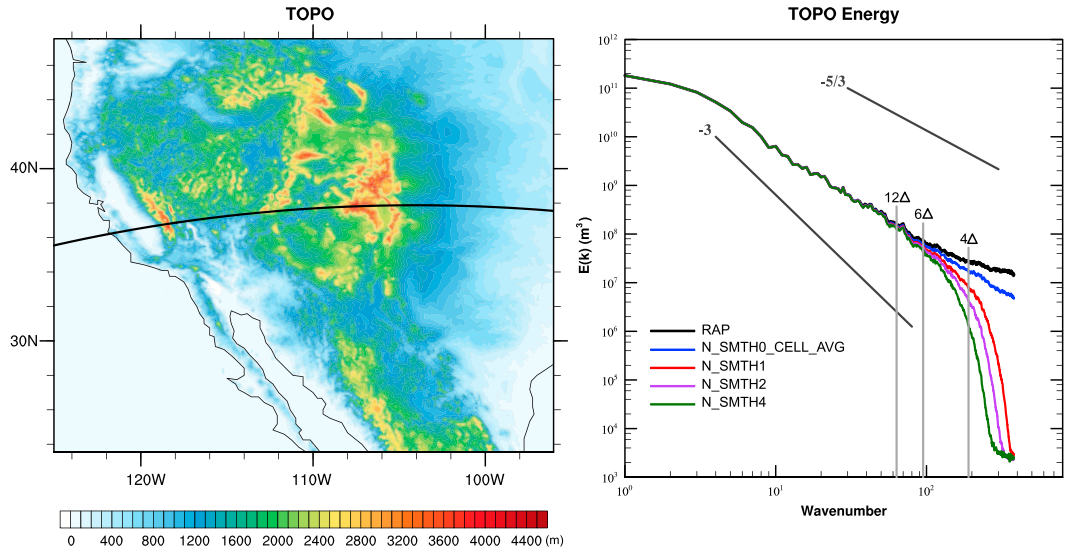

Figure 1. (left) Horizontal distribution of terrain height (color shading; m) in the CTL experiment that is the same as the WRF-RAP system and (right) energy spectra of terrain height as a function of horizontal wavelength and wave number along the cross-section line on the left. A diagonal and three vertical reference lines indicate the representative slopes of $k^{-5/3}$ and different horizontal reference scales ($12\Delta x$, $6\Delta x$, and $4\Delta x$).

example, on 2 November 2015 many reports of smooth (EDR $<$ 0.05) and light (0.05 $<$ EDR $<$ 0.1) turbulence were reported by several commercial aircraft over the western mountainous region of the U.S., in regions where larger areas of light (0.05 $<$ EDR $<$ 0.1) or stronger turbulence (EDR $>$ 0.1) were predicted by the operational system (see Figure 3a). These are presumably linked to terrain and mountain waves, although there are no observations available to verify the magnitude and locations of the mountain waves.

Pursuing this forecasting error further, we found that the operational WRF-RAP system does not include topography smoothing in the model initialization in order to permit inclusion of more realistic small-scale terrain features (S. G. Benjamin, personal communication, 2016). However, this appears to create unrealistically large areas of light-or-stronger turbulence due to the spurious small-scale mountain wave features aloft induced by the unfiltered small-scale energy of the topography (see Figure 3a). In this study, therefore, we tested the WRF model for the same configuration as in the operational WRF-RAP system on the 2 November 2015 case with additional terrain smoothing. We examine the impact of additional terrain smoothing in the initialization of the NWP model on the subsequent reduction of light-or-stronger turbulence forecasts over mountainous regions. In section 2, the design of the experiments and terrain smoothing in the WRF model are introduced. Horizontal and vertical cross sections from different experiments are examined in section 3, and conclusions follow in section 4.

2. Experimental Design of the Model and Terrain Smoothing Method

The current WRF-RAP system uses the Advanced Research version 3.6.1 of the WRF model with hourly update cycles of data assimilation [*Benjamin et al.*, 2016]. In this study, physical packages, domain location, and horizontal and vertical grid spacings are set to the same as the current WRF-RAP system with a 13 km horizontal grid spacing, except that the initial and boundary conditions are forced by 6-hourly National Center for Environmental Prediction/National Center for Atmospheric Research Final reanalysis data with 1° × 1° horizontal grid spacing. This design of the WRF model has been successfully used for previous turbulence case studies with multiple nested domains [e.g., *Trier and Sharman*, 2009; *Trier et al.*, 2010, 2012; *Kim and Chun*, 2010, 2012; *Kim et al.*, 2014, 2015]. For this case study, 18 h of model integration begins at 00:00 UTC 2 November 2015 in all experiments.

In the WRF Pre-processing System (WPS), the original source of high-resolution digital elevation model (DEM) terrain height data is interpolated to the horizontal grid spacing of the NWP model domain. The topography in a subsection of the model domain is shown in Figure 1 (left). Terrain smoothing can be applied to damp

Table 1. Names, Resolution of Source Topography, Interpolation Method, Number of Smoothing Passes, Smoothing Coefficient, Maximum Terrain Height (m), and Maximum of Absolute Vertical Velocity ($m\,s^{-1}$) Along the Cross Section Shown in Figure 2

Name of Exp.	Topo Source	Interp. Method	Smoothing Passes	Max Topo Height (m)	Max. of $\|w\|$ ($m\,s^{-1}$)
CTL (RAP)	2 m	4pts interp.	0	3768.44	4.66
SMTH0	30s	Avg.cell	0	3643.72	3.96
SMTH1	30s	Avg.cell	1	3628.99	2.32
SMTH2	30s	Avg.cell	2	3625.46	1.99
SMTH4	30s	Avg.cell	4	3618.16	1.83

out small-scale topographic features. As already mentioned above, the current WRF-RAP system skips this terrain-smoothing process to leave more realistic small-scale topography in the model, which we argue causes the side effect of overpredicting smooth-to-light turbulence to be stronger over mountainous terrain (see Figure 3a).

In this study, four additional experiments with different levels of additional terrain-averaging procedures are conducted (Table 1). In the control run (hereafter, CTL) that is the same as WRF-RAP system, 2 min (2 m) DEM terrain height data are interpolated to 13 km WRF-RAP domain by a 4-point (4pts) interpolation method. In the four smoothing (SMTH) experiments, 30 s (30s) DEM terrain height and an averaging cell (Avg.cell) interpolation methodology are used for additional averaging of the terrain in WPS. SMTH0, SMTH1, SMTH2, and SMTH4 experiments applied this procedure 0, 1, 2, and 4 times, respectively, using filter equation as

$$h_{i,j}^{n+1} = h_{i,j}^{n} - \alpha \Delta^4 h_{i,j}^{n} \tag{1}$$

where Δ^4 is a two-dimensional fourth-order difference operator as *Guo and Chen* [1994]. Here h is terrain height, $n+1$ is the number of smoothness, i and j are the grid numbers, and α is the coefficient for removing $2\Delta x$ mode and is set to 0.025 for all experiments.

Using the terrain height along the cross section in Figure 1 (left), a one-dimensional fast Fourier transform (FFT) is conducted to produce terrain energy spectra. These spectra, shown in Figure 1 (right), have a $-5/3$ slope when the wavelength (λ) is larger than about 100 km and become shallow for $\lambda \leq 100$ km. In Figure 1 (right), only the unsmoothed terrain is shallower when 4-points interpolation is used from DEM without any filtering (black line). The CTL experiment exhibits significant energy in the smaller scales (~$2\Delta x$). One can argue that these small scales should be damped out in the NWP model because they are unphysical modes. SMTH0 (blue line), cell-averaging interpolation without any filter, has some reduction of the small scales in the energy spectrum, but it does not fully eliminate the unphysical mode. Significant reductions of the energy spectra at small scales are dominant in the SMTH1, SMTH2, and SMTH4 experiments especially energy in the unphysical mode. This implies that the additional terrain-smoothing procedure is important and necessary in the initialization of the NWP model to remove the unphysical energy aloft especially in the smaller scales in the model, which can cause spurious flows in the simulated atmosphere. The maximum terrain height of 3768.44 m across the Sierra Nevada mountain range (cross-section line in Figure 1, right) in the CTL is gradually reduced to 3618.16 m in the SMTH4 experiment (Table 1).

3. Results

Figure 2 shows the simulated vertical velocity and potential temperature from the CTL, SMTH0, SMTH1, and SMTH4 experiments along the cross section in Figure 1. In both the CTL and SMTH0 experiments (Figure 2, top), small-scale spurious wave patterns trapped in each column are especially apparent over the terrain, which are directly induced by the high spectral content of the small-scale topography (Figure 1, right). In the SMTH1 and SMTH4 experiments (Figure 2, bottom), however, unphysical wave patterns are significantly eliminated, while more physically realistic vertical propagation of wave energy with upstream tilted phase lines remain over the significant mountain features. This result strongly suggests that the additional terrain averaging procedure in the initialization of NWP model is important to damp out the unphysical modes especially over the mountainous region. Within increased terrain smoothing, the maximum of $|w|$ ($4.66\,m\,s^{-1}$) in the CTL is significantly decreased to $1.83\,m\,s^{-1}$ in the SMTH4 experiment (Table 1).

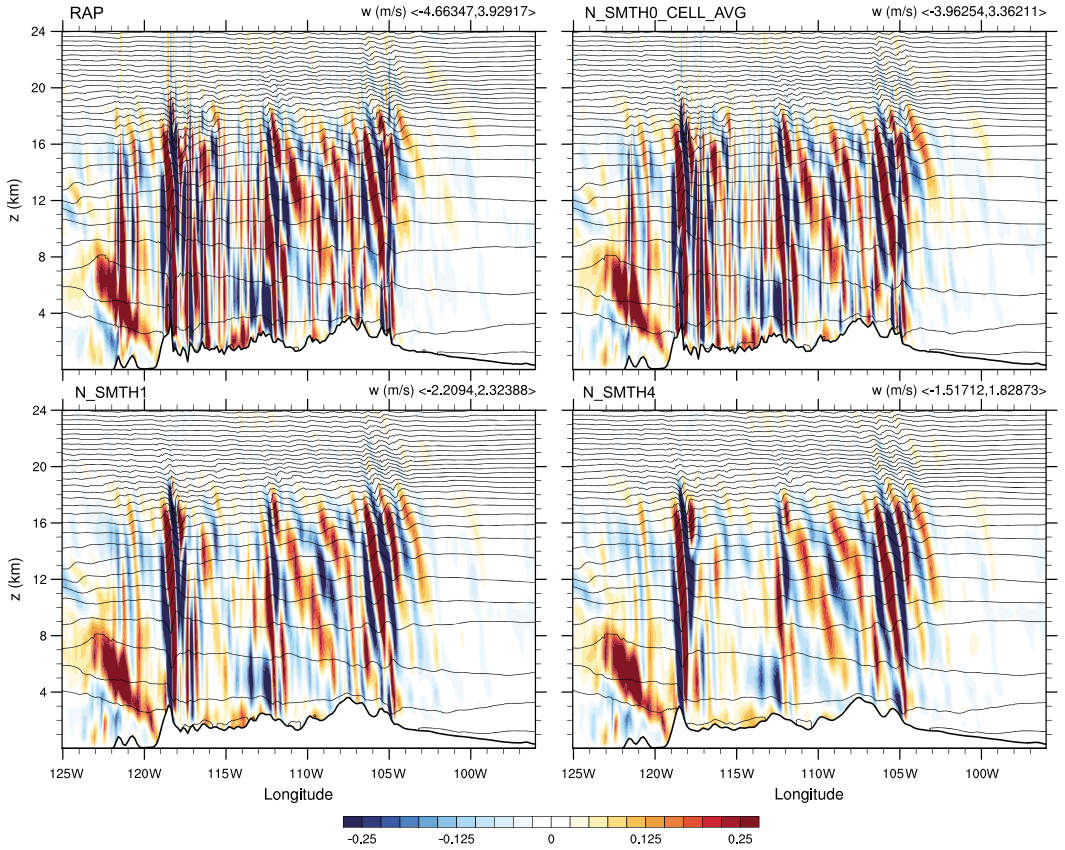

Figure 2. Vertical cross sections for vertical velocity (shading), potential temperature with 4 K contour interval, and terrain height along the cross-section line shown in Figure 1 (left), derived from CTL experiment using the (top left) WRF-RAP configuration, (top right) SMTH0, (bottom left) SMTH1, and (bottom right) SMTH4 experiments in Table 1.

The current operational GTG system has three steps. First, it calculates several turbulence diagnostics using NWP model output. One of them is $|w|/Ri$, where w is vertical velocity and Ri is Richardson number, the dimensionless ratio between stability and vertical wind shear. $|w|/Ri$ is especially important for MWT, because the combination of vertical velocity and Ri captures both mountain waves and environmentally unstable regions where mountain waves can either break down or enhance local background shear and stability, generating small-scale turbulence [e.g., *Lane et al.*, 2009; *Kim and Chun*, 2010; *Sharman et al.*, 2011]. Second, various numerical units and magnitudes from individual turbulence diagnostics like $|w|/Ri$ ($\mathrm{m\,s^{-1}}$) are converted into a EDR scale ($\mathrm{m^{2/3}\,s^{-1}}$) by using a simple equation [$\log \mathrm{EDR}(x, y, z) = a + b \log D_i(x, y, z)$, where D_i is the raw diagnostic value and a and b are derived from the mean and standard deviation of a lognormal fit to the long-term probability density function of in situ aircraft observations [*Sharman et al.*, 2014a, 2014b; *Kim et al.*, 2015]. Motivation of this EDR mapping is that it represents the magnitude of atmospheric turbulence directly affecting aircraft and is consistent with observed in situ EDR that is current standard by *International Civil Aviation Organization* [2010]. Using predefined a and b parameters, the raw values of $|w|/Ri$ ($\mathrm{m\,s^{-1}}$) are mapped into EDR ($\mathrm{m^{2/3}\,s^{-1}}$), which is plotted in Figure 3. Third, GTG combines individual diagnostics to an optimal EDR-scale turbulence product using weighted scoring functions based on their forecast performance against observations. $|w|/Ri$ is one of more useful MWT diagnostics in the current system [*Sharman et al.*, 2014a].

Figure 3 shows the snapshot of EDR converted from $|w|/Ri$ at 35,000 ft (FL350; about z = 10,668 m) from four simulations (CTL, SMTH0, SMTH1, and SMTH4) along with observed in situ EDR and pilot report (PIREP) data. In this case, a high-amplitude upper level trough is located over the Pacific coast, and an anticyclonically curved jet stream is apparent over northern California, eastern Oregon, northern Idaho, and western Montana, which is consistent with reanalysis and observations (not shown). This contributes to relatively

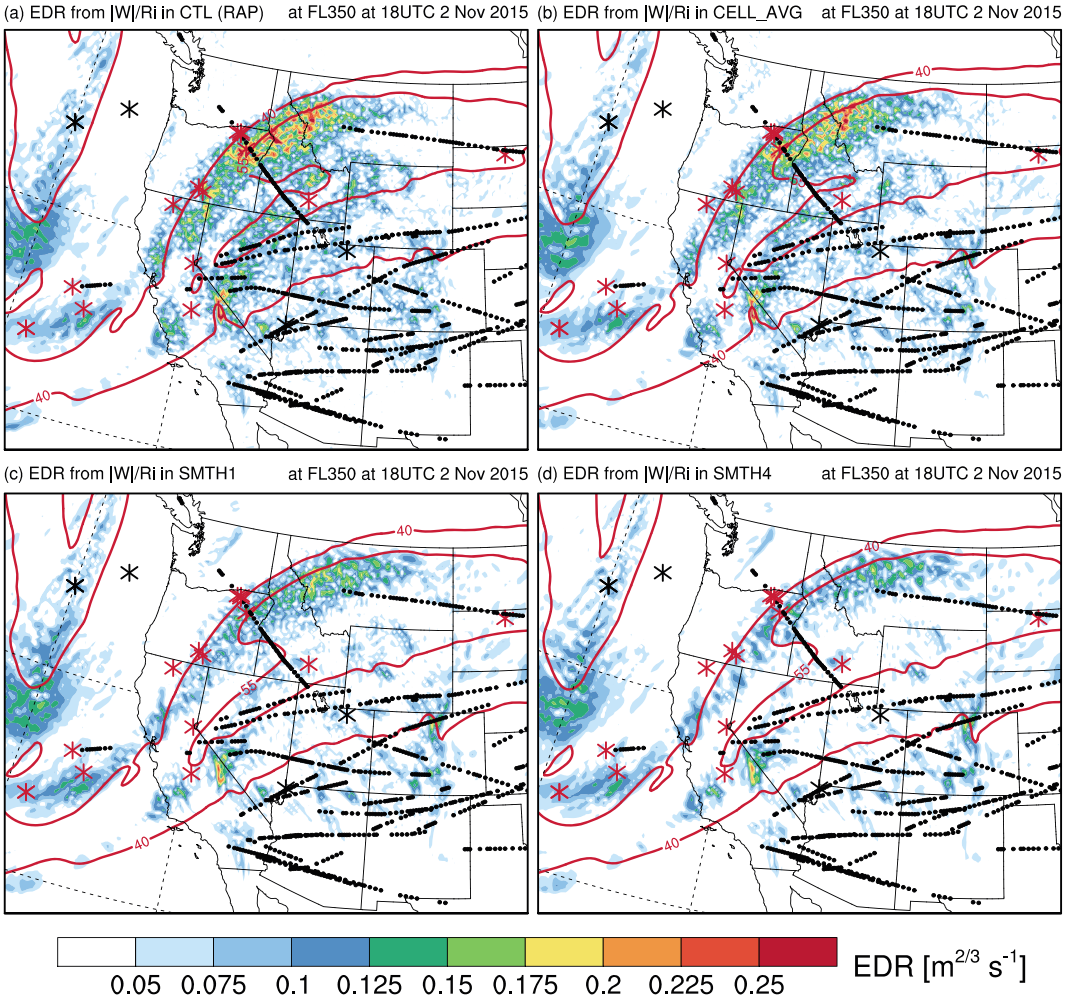

Figure 3. Color shadings of the eddy dissipation rate (EDR; $m^{2/3}\ s^{-1}$) turbulence forecasts derived and converted from $|w|/Ri$, where w is vertical velocity and Ri is Richardson number $Ri = N^2/VWS^2$, where N^2 is the Brunt-Väisälä frequency and VWS is the vertical wind shear, and red contours of horizontal wind speed (40 and 55 m s^{-1}) valid at 18:00 UTC 2 November 2015 from (a) CTL, (b) SMTH0, (c) SMTH1, and (d) SMTH4 experiments. Observed in situ EDR and smooth pilot reports (PIREPs) corresponding to EDR < 0.05 at ± 2 h around 18:00 UTC and $\pm$ 2500 ft (762 m) around 35,000 ft (FL350; z = 10,668 m) are depicted as black dots and asterisks, respectively. Light intensity of in situ EDR and PIREP observations corresponding to $0.05 <$ EDR < 0.1 are indicated with red asterisks.

higher values of forecasted EDR especially in the cyclonic shear side of the jet stream and localized mountain waves aloft. During this period, most of observed in situ EDR is smooth (EDR < 0.05; black dots). And, PIREPs shown as black and red asterisks are only reported as smooth and light turbulence occasionally. However, larger areas of light ($0.05 <$ EDR < 0.1) or stronger (EDR > 0.1) values appear more in the CTL and SMTH0 experiments (Figures 3a and 3b) than SMTH1 and SMTH4 experiments (Figures 3c and 3d). This discrepancy is mainly because the additional terrain-averaging procedures in the SMTH1 and SMTH4 wash out the unphysical energy from the unfiltered small-scale terrain (Figure 1) and reduce spurious waves over the mountainous regions (Figure 2). In SMTH1 and SMTH4 (Figures 3c and 3d), the smoothing significantly reduces unrealistically large areas of light-or-stronger turbulence forecasts over the mountainous region. This is more consistent with actual smooth-to-light turbulence observed by commercial aircraft (Figures 3c and 3d).

There are some additional interesting features in Figure 3. First, the structure and position of the large-scale upper level jet stream shown as red contours are almost identical in all experiments, implying that additional terrain smoothing does not affect the large-scale atmospheric environment but eliminates the small-scale spurious trapped mountain waves shown in Figure 2. Second, from all four experiments magnitude and

structure of the EDR forecasts over the Pacific Ocean are almost identical and consistent with observation (asterisks), which means that the additional damping only affects EDR forecasts over the western mountain regions. Third, there were some light turbulence reports ($0.05 < \mathrm{EDR} < 0.1$; red asterisks) over the Sierra-Nevada range. But, those are not exactly near the significant wave region along the California/Nevada border. It might be possible that commercial already avoided this high potential area of strong turbulence in the steep wave region or that there were no flights over this region at that time. Fourth, there were some smooth EDR (black dots) and light PIREPs (red asterisks) across Oregon and Idaho, where large areas of stronger turbulence are forecasted in the CTL experiment (Figure 3a). Again, white background ($\mathrm{EDR} < 0.05$) and blue shadings of EDR forecasts ($0.05 < \mathrm{EDR} < 0.1$) in the SMTH experiments (Figures 3c and 3d) indicate that the smoothing washes out stronger turbulence features in the CTL run (Figure 3a) and is much more consistent with actual in situ EDR and PIREP observations of smooth ($\mathrm{EDR} < 0.05$) and light ($0.05 < \mathrm{EDR} < 0.1$) turbulence reports.

4. Conclusions

The motivation of this study is to investigate the unrealistically large areas of elevated turbulence forecasts over the western mountainous region of U.S. in the current operational system. This study simulates the atmospheric environment over the Western mountainous region using the current operational design of the WRF-RAP NWP model for the 2 November 2015 case, when the CTL model forecasts a high potential of stronger upper level turbulence but only smooth-to-light turbulence reports were received from on-board turbulence measurements from commercial aircraft. From the FFT analyses along the high mountain region in the CTL, high energy is included in the smaller scales ($\sim 2\Delta x$) of the spectrum, which is unphysical and should be damped out by numerical smoothing. Additional SMTH experiments with different levels of additional terrain-averaging in the model initialization show that the large and mesoscale energy spectra are almost identical to the CTL, but there is a significant reduction of energy near the grid scale, which reduces turbulence forecast intensity over that region. This is consistent with the observational data for this case. The results strongly suggest that the additional terrain averaging is beneficial in the initialization of the NWP model to reduce spurious wave-like patterns trapped in each model column, and would enhance the performance of operational turbulence forecasts. This study only focuses on the impact of the terrain averaging on aviation turbulence forecasts. However, it remains to be seen whether the additional terrain smoothing may produce better low-level wind and temperature forecasts over the mountainous regions as well.

Acknowledgments

This research is in response to requirements and funding by the U.S. Federal Aviation Administration (FAA). The views expressed are those of the authors and do not necessarily represent the official policy and position of the FAA. Authors very thank Melissa A. Thomas at Delta Air Lines for her observation of large areas of smooth-to-light turbulence forecasts over the western U.S. mountainous regions. The authors also thank Stanley G. Benjamin at NOAA/ESRL for his feedback on this issue. The authors thank two anonymous reviewers for their invaluable comments and suggestions.

References

Benjamin, S. G., et al. (2016), A North American hourly assimilation and model forecast cycle: The Rapid Refresh, *Mon. Weather Rev.*, *144*(4), 1669–1694, doi:10.1175/MWR-D-15-0242.1.

Dutton, J. A., and H. A. Panofsky (1970), Clear air turbulence: A mystery may be unfolding, *Science*, *167*(3920), 937–944, doi:10.1126/science.167.3920.937.

Ellrod, G. P., and D. I. Knapp (1992), An objective Clear-Air Turbulence forecasting technique: Verification and operational use, *Weather Forecast.*, *7*(1), 150–165, doi:10.1175/1520-0434(1992)007<0150:aocatf>2.0.co;2.

Endlich, R. M. (1964), The mesoscale structure of some regions of Clear-Air Turbulence, *J. Appl. Meteorol.*, *3*(3), 261–276, doi:10.1175/1520-0450(1964)003<0261:tmsosr>2.0.co;2.

Guo, Y.-R., and S. Chen (1994), Terrain and land use for the fifth-generation Pen State/NCAR mesoscale modeling system (MM5): Program TERRAIN, *NCAR Tech. Note NCAR/TN-397 + IA*.

International Civil Aviation Organization (2010), Meteorological service for international air navigation. Annex 3 to the Convention on International Civil Aviation, 17th ed., ICAO International Standards and Recommended Practices Tech. Annex, 206 pp.

Kim, J.-H., and H.-Y. Chun (2010), A numerical study of Clear-Air Turbulence (CAT) encounters over South Korea on 2 April 2007, *J. Appl. Meteorol. Climatol.*, *49*(12), 2381–2403, doi:10.1175/2010jamc2449.1.

Kim, J.-H., and H.-Y. Chun (2011), Statistics and possible sources of aviation turbulence over South Korea, *J. Appl. Meteorol. Climatol.*, *50*(2), 311–324, doi:10.1175/2010jamc2492.1.

Kim, J.-H., and H.-Y. Chun (2012), A numerical simulation of convectively induced turbulence above deep convection, *J. Appl. Meteorol. Climatol.*, *51*(6), 1180–1200, doi:10.1175/jamc-d-11-0140.1.

Kim, J.-H., H.-Y. Chun, R. D. Sharman, and T. L. Keller (2011), Evaluations of upper-level turbulence diagnostics performance using the Graphical Turbulence Guidance (GTG) system and pilot reports (PIREPs) over East Asia, *J. Appl. Meteorol. Climatol.*, *50*(9), 1936–1951, doi:10.1175/jamc-d-10-05017.1.

Kim, J.-H., H.-Y. Chun, R. D. Sharman, and S. B. Trier (2014), The role of vertical shear on aviation turbulence within cirrus bands of a simulated western Pacific cyclone, *Mon. Weather Rev.*, *142*(8), 2794–2813, doi:10.1175/MWR-D-14-00008.1.

Kim, J.-H., W. N. Chan, B. Sridhar, and R. D. Sharman (2015), Combined winds and turbulence prediction system for automated air-traffic management applications, *J. Appl. Meteorol. Climatol.*, *54*(4), 766–784, doi:10.1175/jamc-d-14-0216.1.

Kim, J.-H., W. N. Chan, B. Sridhar, R. D. Sharman, P. D. Williams, and M. Strahan (2016), Impact of the North Atlantic Oscillation on transatlantic flight routes and Clear-Air Turbulence, *J. Appl. Meteorol. Climatol.*, *55*(3), 763–771, doi:10.1175/JAMC-D-15-0261.1.

Knox, J. A., D. W. McCann, and P. D. Williams (2008), Application of the Lighthill-Ford Theory of spontaneous imbalance to Clear-Air Turbulence forecasting, *J. Atmos. Sci.*, *65*(10), 3292–3304, doi:10.1175/2008jas2477.1.

Lane, T. P., J. D. Doyle, R. D. Sharman, M. A. Shapiro, and C. D. Watson (2009), Statistics and dynamics of aircraft encounters of turbulence over Greenland, *Mon. Weather Rev.*, *137*(8), 2687–2702, doi:10.1175/2009mwr2878.1.

Lane, T. P., R. D. Sharman, S. B. Trier, R. G. Fovell, and J. K. Williams (2012), Recent advances in the understanding of near-cloud turbulence, *Bull. Am. Meteorol. Soc.*, *93*(4), 499–515, doi:10.1175/bams-d-11-00062.1.

Lindborg, E. (2007), Horizontal wavenumber spectra of vertical vorticity and horizontal divergence in the upper troposphere and lower stratosphere, *J. Atmos. Sci.*, *64*(3), 1017–1025, doi:10.1175/JAS3864.1.

Shapiro, M. A. (1980), Turbulent mixing within tropopause folds as a mechanism for the exchange of chemical constituents between the stratosphere and troposphere, *J. Atmos. Sci.*, *37*(5), 994–1004, doi:10.1175/1520-0469(1980)037<0994:tmwtfa>2.0.co;2.

Sharman, R. D., C. Tebaldi, G. Wiener, and J. Wolff (2006), An integrated approach to mid- and upper-level turbulence forecasting, *Weather Forecasting*, *21*(3), 268–287, doi:10.1175/waf924.1.

Sharman, R. D., J. D. Doyle, and M. A. Shapiro (2011), An investigation of a commercial aircraft encounter with severe Clear-Air Turbulence over western Greenland, *J. Appl. Meteorol. Climatol.*, *51*(1), 42–53, doi:10.1175/jamc-d-11-044.1.

Sharman, R. D., S. B. Trier, T. P. Lane, and J. D. Doyle (2012), Sources and dynamics of turbulence in the upper troposphere and lower stratosphere: A review, *Geophys. Res. Lett.*, *39*, L12803, doi:10.1029/2012gl051996.

Sharman, R. D., J. Pearson, G. Wiener, and J. Prestopnik (2014a), Technical description document (TDD) for the Graphical Turbulence Guidance Product v3.0 (GTG3.0). FAA AWRP Turbulence PDT, 26 pp.

Sharman, R. D., L. B. Cornman, G. Meymaris, J. Pearson, and T. Farrar (2014b), Description and derived climatologies of automated in situ eddy-dissipation-rate reports of atmospheric turbulence, *J. Appl. Meteorol. Climatol.*, *53*(6), 1416–1432, doi:10.1175/jamc-d-13-0329.1.

Skamarock, W. C., J. Klemp, J. Dudhia, D. Gill, D. Barker, W. Wang, X.-Y. Huang, M. Duda, and J. Powers (2008), A description of the Advanced Research WRF version 3, *NCAR Tech. Note NCAR/TN-4751STR*, 113 pp. [Available online at http:// www.mmm.ucar.edu/wrf/users/docs/arw_v3_bw.pdf.]

Trier, S. B., and R. D. Sharman (2009), Convection-permitting simulations of the environment supporting widespread turbulence within the upper-level outflow of a mesoscale convective system, *Mon. Weather Rev.*, *137*(6), 1972–1990, doi:10.1175/2008mwr2770.1.

Trier, S. B., R. D. Sharman, R. G. Fovell, and R. G. Frehlich (2010), Numerical simulation of radial cloud bands within the upper-level outflow of an observed mesoscale convective system, *J. Atmos. Sci.*, *67*(9), 2990–2999, doi:10.1175/2010jas3531.1.

Trier, S. B., R. D. Sharman, and T. P. Lane (2012), Influences of moist convection on a cold-season outbreak of Clear-Air Turbulence (CAT), *Mon. Weather Rev.*, *140*(8), 2477–2496, doi:10.1175/mwr-d-11-00353.1.